# Calibration of Catadioptric Sensors by Polarization Imaging

Olivier Morel and David Fofi

***Abstract*— A new efficient method of calibration for catadioptric sensors is presented in this paper. It is based on an accurate reconstruction of the mirror by means of polarization imaging and it permits to relax most of the constraints related to the calibration of the catadioptric systems. No image processing and no calibration pattern are required so that the calibration can be performed in "one click". As a result, the coordinates of the projection rays and a mapping between projection rays and image pixels is obtained. Besides, two methods of triangulation have been adapted to catadioptric sensors and tested. Experiments prove the validity of the method with some preliminary results on 3D reconstruction.**

## I. Introduction

COMMON calibration methods for omnidirectional catadioptric sensors assume that: *(i)* the mirror shape is perfectly known; *(ii)* the alignment of the sensor is perfect so that the single viewpoint constraint is satisfied; *(iii)* the projection model can be easily parameterized. Some methods relax the second constraint and a few relax the first, but before some recent works [1], [2], [3] calibrating methods always underlie an explicit parametric model of projection.

How can a camera be defined, as generally as possible? A camera captures light that travel along a ray in space. Each ray forms a pixel onto the image plane. Therefore, according to Sturm, a camera is completely described by:

- the coordinates of the projection rays;
- the mapping between rays and pixels.

This model has the advantage of working for any type of camera (catadioptric systems, central cameras with or without distorsion, axial cameras, etc.) and to handle heterogeneous systems [4] (for instance, a sensor composed of an omnidirectional camera and a perspective camera). However, developing an efficient and easy-to-use calibration method based on this model is not trivial. In this paper, a new method is proposed that permits to calibrate a catadioptric sensor by polarization imaging, relaxing the three constraints listed above. Moreover, the calibration can be performed even by a non-specialist as it only requires an optical apparatus and no image processing. In addition, two methods of triangulation adapted to this general model (pixel-ray model) are presented.

The article is structured as follows. Next section presents some basic knowledge about polarization imaging. Then, the calibration method and the two methods of triangulation are detailed. Some experimental results are given in section 5; the method is validated and discussed. Finally, the paper ends with a conclusion and a word about future work to be undertaken.

This work was supported by the A.N.R. ("Agence Nationale de la Recherche"), Ca.Vi.A.R. (Catadioptric Vision of Aerial Robots), project n°NT05-2_41786. Website: http://www.anr-caviar.org/.

O. Morel and D. Fofi are with the Le2i, Laboratory of Electronics, Computer Science and Image, UMR CNRS 5158, 71200 Le Creusot, France (e-mail: d.fofi@iutlecreusot.u-bourgogne.fr).

## II. Polarization Imaging

Polarization imaging enables to study the polarization state of a light wave. The most common applications in artificial vision are the abilities to distinguish objects of dielectric and metallic nature [5] and to detect transparent surfaces. Polarization imaging enables likewise to give three-dimensional information of the specular objects: the so called "Shape from polarization" method. The physical principle is the following: after being reflected, an unpolarized light wave becomes partially linearly polarized, depending on the surface normal and on the refractive index of the media it impinges on. A partially linearly polarized light has three parameters: the light magnitude $I$, the degree of polarization $\rho$ and the angle of polarization $\varphi$.

To calibrate the mirror used in our catadioptric sensor, the polarization state of the reflected light has to be measured. In order to get unpolarized light, the complete sensor is just put in a sheet of paper cylinder (Fig. 1). Since the reflected light is partially linearly polarized, the use of a rotating polarizer between the camera and the mirror is enough. Each intensity light of the pixels is linked to the angle of the polarizer and to the polarization parameters by the following equation:

$$I_p(\alpha) = \frac{I}{2}\left(\rho\cos\left(2\alpha - 2\varphi\right) + 1\right), \qquad (1)$$

where $\alpha$ is the polarizer angle. The purpose of polarization imaging is to compute the three parameters, $I$, $\varphi$, and $\rho$, by interpolating this formula. Because there are three parameters, at least three images, taken with different orientations of the polarizer, are required. To get an automatic calibration of the catadioptric system, a liquid-crystal polarization rotator is used instead of the polarizer. It acts as a rotating polarizer, which has the ability to be electrically controlled. Fig 2 shows the image of the degree and angle parameters of a hemispheric mirror.

### A. Relationship between the polarization parameters and the normals

Wolff and Boult have demonstrated how to determine constraints on surface normals by using the Fresnel reflectance model [6]. The surface of the mirror is assumed to be continuous and described by a Cartesian expression: $z = f(x, y)$. Therefore, each surface normal is given by the following non-normalized expression:

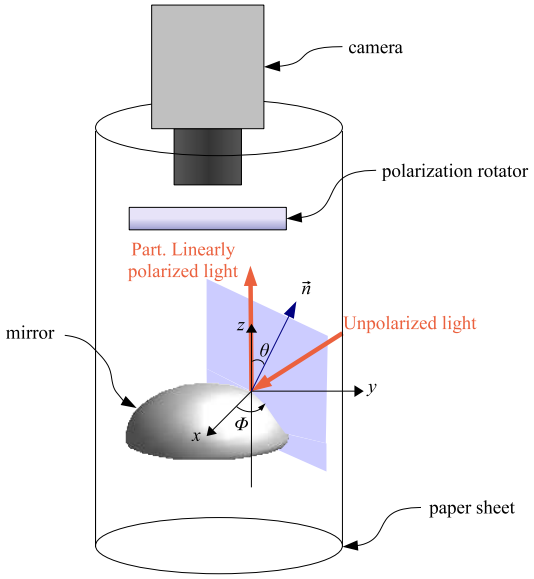


Fig. 1. Polarization imaging: after being reflected by the mirror, the light becomes partially linearly polarized.

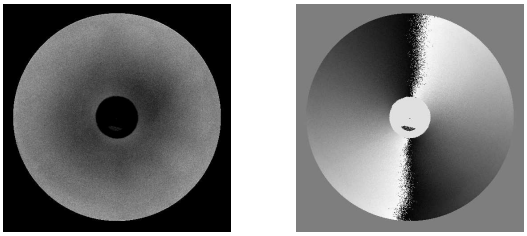

(a) (b)

Fig. 2. Images of the polarization parameters that are needed to reconstruct the mirror shape: (a) degree of polarization ($\rho \in [0,1]$), (b) angle of polarization ($\varphi \in [0,\pi]$).

$$\vec{n} = \begin{bmatrix} -\frac{\partial f(x,y)}{\partial x} \\ -\frac{\partial f(x,y)}{\partial y} \\ 1 \end{bmatrix} = \begin{bmatrix} p = \tan\theta\cos\phi \\ q = \tan\theta\sin\phi \\ 1 \end{bmatrix}. \quad (2)$$

The aim of "Shape from polarization" is to compute the normals from the angles $\theta$ and $\phi$. By combining Fresnel formulas and the Snell-Descartes law one can find a relationship between the degree of polarization $\rho$ and the zenith angle $\theta$ [7]. For specular metallic surfaces, the following formula can be applied [8]:

$$\rho(\theta) = \frac{2n\tan\theta\sin\theta}{\tan^2\theta\sin^2\theta + |\hat{n}|^2}, \quad (3)$$

where $\hat{n} = n(1+i\kappa)$ is the complex refractive index of the mirror.

The azimuth angle $\phi$ is linked to the angle of polarization $\varphi$ since the reflected light becomes partially linearly polarized according to the normal of the plane of incidence. Because our imaging system uses a telecentric lens, orthographic projection onto the sensor is assumed and the azimuth angle $\phi$ can be inferred from the angle of

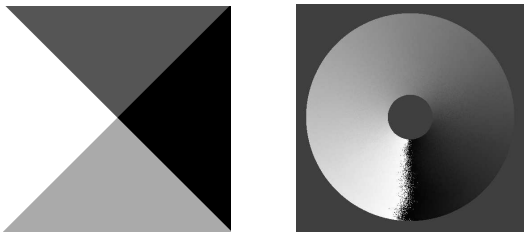

(a) (b)

Fig. 3. Disambiguation of the azimuth angle: (a) segmented image ($I_{quad} \in \{0,1,2,3\}$), (b) image of the resulting azimuth angle $\phi$ ($\phi \in [-\pi/2, 3\pi/2]$).

polarization $\varphi$:

$$\phi = \varphi \pm \frac{\pi}{2}. \quad (4)$$

### B. Disambiguation of the normals

From the equations (3) and (4) the surface normals are determined with an ambiguity. Since the mirrors used in catadioptric vision are of convex and revolution shape, a segmented image $I_{quad}$ can be directly computed from the near center of the mirror (Fig. 3(a)). This segmented image is an image with four gray levels that represent the four quadrants oriented with an angle in $]0, \pi/2[$. The algorithm of the disambiguation process described in [9] is applied with the segmented image $I_{quad}$ and the angle of polarization image $\varphi$:

1) $\phi = \varphi - \frac{\pi}{2}$,
2) $\phi = \phi + \pi$ if $[(I_{quad} = 0) \wedge (\phi \leq 0)] \vee [I_{quad} = 1] \vee [(I_{quad} = 3) \wedge (\phi \geq 0)]$,

where $\wedge$ and $\vee$ represent, respectively, the logical operators AND and OR. The result of the disambiguation is presented Fig. 3(b).

## III. Mirror Calibration

To calibrate our imaging system, we use the generic calibration concept introduced by Sturm and Ramalingam [10]. The concept considers an image as a collection of pixels, and each pixel measures the light along a particular 3D ray. Thus, calibration is the determination of the coordinates of all pixels' rays. A 3D-ray is represented here by a couple of points which belongs to the ray:

$$\mathbf{A} = \begin{bmatrix} x_a \\ y_a \\ z_a \end{bmatrix}, \mathbf{B} = \begin{bmatrix} x_b \\ y_b \\ z_b \end{bmatrix}. \quad (5)$$

To get these points, the 3D surface of the mirror has to be computed. Once the normals are given by polarization imaging, the surface shape of the mirror can be computed thanks to the Frankot-Chellappa algorithm [11]. Denoting by $\tilde{f}$, $\tilde{p}$ and $\tilde{q}$ the Fourier transforms of, respectively, the surface height and the $x$, $y$ gradients, we have:

$$\forall\,(u,v) \neq (0,0)\,,\ \tilde{f}(u,v) = \frac{-ju\tilde{p} - jv\tilde{q}}{u^2+v^2}. \quad (6)$$

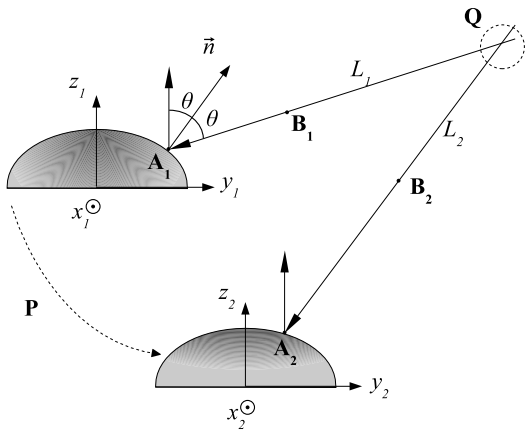


Fig. 4. Description of the 3D point reconstruction by triangulation of the projection rays.

The three-dimensional surface is obtained by taking the inverse Fourier transform of the former equation. This integration process gives us the surface height of the mirror with a constant of integration. Nevertheless, this constant is not required since the orthographic projection is assumed. To calibrate the sensor, let take the point $\mathbf{A} = [x, y, z]^T$, that both belongs to the mirror surface and the 3D-ray, be the first point of the ray (Fig. 4). The second point $\mathbf{B}$ of the ray can be written as:

$$\mathbf{B} = \mathbf{A} + k \begin{bmatrix} \tan 2\theta \cos\phi \\ \tan 2\theta \sin\phi \\ 1 \end{bmatrix}, \tag{7}$$

where $k$ is a non-null constant.

## IV. Triangulation

Once the sensor is calibrated, and assuming that the motion between two camera shots is known, it is possible to reconstruct 3D scenes by triangulating the projection rays. Two methods, known in the literature [12] as *Linear-Eigen* and *Mid-Point*, have been adapted to the pixel-ray model. *Camera 1* (resp. *camera 2*) will denote the first (resp. second) camera of a stereovision system or, alternatively, the first (resp. second) view of a monocular system in motion.

### A. Linear-Eigen Method

Let us assume two points $\mathbf{A}_1$ and $\mathbf{B}_1$ belonging to one projection ray (attached to camera 1) and two other points $\mathbf{A}_2$ and $\mathbf{B}_2$ belonging to a second projection ray (attached to camera 2). If the two projection rays match, they will intersect to a point $\mathbf{Q}$ in space (Fig. 4). It is well known that any point $\mathbf{Q}$ belonging to a line in space may be expressed by a linear combination of two other points of the line (assuming that camera 1 is set to the origin):

$$\mathbf{Q} = \lambda_1 \mathbf{A}_1 + \mu_1 \mathbf{B}_1 \tag{8}$$

Let $\mathbf{P} = \begin{bmatrix} \mathbf{R} & \mathbf{t} \\ \mathbf{0} & 1 \end{bmatrix}$ be the pose matrix of the camera 2, i.e. the motion between camera 2 and camera 1, then:

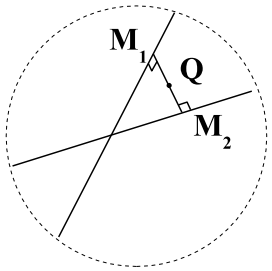


Fig. 5. Zoom of Fig. 4: in the Mid-Point method, the triangulated point $\mathbf{Q}$ is the barycenter of $\mathbf{M_1}$ and $\mathbf{M_2}$.

$$\mathbf{PQ} = \lambda_2 \mathbf{A}_2 + \mu_2 \mathbf{B}_2. \tag{9}$$

By grouping (8) and (9) in a compact form, it is obtained:

$$\forall i = 1, 2 \quad \lambda_i \mathbf{A}_i + \mu_i \mathbf{B}_i = \mathbf{P}_i \mathbf{Q} \tag{10}$$

with $\mathbf{P_1} = \mathbf{I}_{4\times4}$ and $\mathbf{P}_2 = \mathbf{P}$. Finally, this set of equations can be expressed in a matrix form:

$$\begin{bmatrix} \mathbf{I} & \mathbf{A}_1 & \mathbf{B}_1 & \mathbf{0} & \mathbf{0} \\ \mathbf{P} & \mathbf{0} & \mathbf{0} & \mathbf{A}_2 & \mathbf{B}_2 \end{bmatrix} \begin{bmatrix} \mathbf{Q} \\ -\lambda_1 \\ -\mu_1 \\ -\lambda_2 \\ -\mu_2 \end{bmatrix} = 0. \tag{11}$$

This method can be easily generalized to *n* views, leading to:

$$\mathbf{Hx} = \begin{bmatrix} 0 \\ \vdots \\ 0 \end{bmatrix}, \tag{12}$$

where $\mathbf{x} = [\mathbf{Q}, -\lambda_1, -\mu_1, \cdots, -\lambda_n, \mu_n]^T$ and:

$$\mathbf{H} = \begin{bmatrix} \mathbf{P}_1 & \mathbf{A}_1 & \mathbf{B}_1 & 0 & 0 & \cdots & 0 & 0 \\ \mathbf{P}_2 & 0 & 0 & \mathbf{A}_2 & \mathbf{B}_2 & \cdots & 0 & 0 \\ \vdots & \vdots & \vdots & \vdots & \vdots & \ddots & \vdots & \vdots \\ \mathbf{P}_n & 0 & 0 & 0 & 0 & \cdots & \mathbf{A}_n & \mathbf{B}_n \end{bmatrix}.$$

This can be solved by minimizing $\|\mathbf{Hx}\|$ subject to the condition $\|\mathbf{x}\| = 1$. The solution is the unit eigenvector corresponding to the smallest eigenvalue of the matrix $\mathbf{H}^T\mathbf{H}$.

### B. Mid-Point Method

Let $(\mathbf{A}_1, \mathbf{B}_1)$ and $(\mathbf{A}_2, \mathbf{B}_2)$ be pairs of points belonging to the projection rays $L_1$ and $L_2$ respectively. As before, $L_1$ is attached to camera 1, $L_2$ is attached to camera 2 and $\mathbf{P}$ is the pose matrix of the camera 2. In the Mid-Point method, the triangulated point $\mathbf{Q}$ is the barycenter of $\mathbf{M}_1$ and $\mathbf{M}_2$ built as the orthogonal projection of $\mathbf{Q}$ onto the rays $L_1$ and $L_2$ (5). The following relationships can be established:

$$\begin{cases} \overrightarrow{\mathbf{M}_1\mathbf{Q}} \cdot \overrightarrow{\mathbf{A}_1\mathbf{B}_1} = 0 \\ \overrightarrow{\mathbf{M}_2\mathbf{Q}} \cdot \overrightarrow{\mathbf{A}_2\mathbf{B}_2} = 0 \\ \overrightarrow{\mathbf{QM}_1} + \overrightarrow{\mathbf{QM}_2} = \vec{0} \end{cases} \tag{13}$$

Since the points $\mathbf{M}_1$ and $\mathbf{M}_2$ lay on $L_1$ and $L_2$ respectively, it can be written:

$$\begin{cases} \mathbf{M}_1 = \mathbf{A}_1 + \mu_1(\mathbf{B}_1 - \mathbf{A}_1) \\ \mathbf{M}_2 = \mathbf{A}_2 + \mu_2(\mathbf{B}_2 - \mathbf{A}_2) \end{cases} \tag{14}$$

by introducing the position parameters $\mu_i$. Relationships (13) can now be re-arranged as:

$$\begin{cases} (\mathbf{Q} - \mathbf{M}_1)^T(\mathbf{B}_1 - \mathbf{A}_1) = 0 \\ (\mathbf{PQ} - \mathbf{M}_2)^T(\mathbf{B}_2 - \mathbf{A}_2) = 0 \\ \mathbf{M}_1 + \mathbf{P}^{-1}\mathbf{M}_2 = 2\mathbf{Q} \end{cases} \tag{15}$$

Injecting (14) into (15) leads to:

$$\begin{cases} \mathbf{A}_1^T(\mathbf{B}_1 - \mathbf{A}_1) = (\mathbf{B}_1 - \mathbf{A}_1)^T\mathbf{Q} - \mu_1 \left\|\mathbf{B}_1 - \mathbf{A}_1\right\|^2 \\ \mathbf{A}_2^T(\mathbf{B}_2 - \mathbf{A}_2) = (\mathbf{B}_2 - \mathbf{A}_2)^T\mathbf{PQ} - \mu_2 \left\|\mathbf{B}_2 - \mathbf{A}_2\right\|^2 \\ \mathbf{A}_1 + \mathbf{P}^{-1}\mathbf{A}_2 = 2\mathbf{Q} - \mu_1(\mathbf{B}_1 - \mathbf{A}_1) - \mu_2\mathbf{P}^{-1}(\mathbf{B}_2 - \mathbf{A}_2) \end{cases} \tag{16}$$

Finally, this set of equations can be rewritten into matricial form:

$$\begin{bmatrix} \mathbf{A}_1^T(\mathbf{B}_1 - \mathbf{A}_1) \\ \mathbf{A}_2^T(\mathbf{B}_2 - \mathbf{A}_2) \\ \mathbf{A}_1 + \mathbf{P}^{-1}\mathbf{A}_2 \end{bmatrix} = \mathbf{K} \begin{bmatrix} \mathbf{Q} \\ \mu_1 \\ \mu_2 \end{bmatrix}, \tag{17}$$

with $\mathbf{K} = \begin{bmatrix} (\mathbf{B}_1 - \mathbf{A}_1)^T & -\left\|\mathbf{B}_1 - \mathbf{A}_1\right\|^2 & 0 \\ (\mathbf{B}_2 - \mathbf{A}_2)^T\mathbf{P} & 0 & -\left\|\mathbf{B}_2 - \mathbf{A}_2\right\|^2 \\ 2\mathbf{I} & -(\mathbf{B}_1 - \mathbf{A}_1) & -\mathbf{P}^{-1}(\mathbf{B}_2 - \mathbf{A}_2) \end{bmatrix}$, and where $\mathbf{I}$ is the $3 \times 3$ identity matrix.

This method can be generalized as well to $n$ views. Let us assume pairs of points $(\mathbf{A}_i, \mathbf{B}_i)$ and $\mathbf{M}_i$ expressed in the coordinates frame attached to the camera $i$ whose pose matrix is denoted by $\mathbf{P}_i$. Let us consider $\mathbf{Q}$ the triangulated point as expressed in the world coordinates frame. This yields:

$$\begin{cases} \forall i \in [1, n],\ (\mathbf{P}_i\mathbf{Q} - \mathbf{M}_i)^T(\mathbf{B}_i - \mathbf{A}_i) = 0 \\ \forall i \in [1, n],\ \mathbf{M}_i = \mathbf{A}_i + \mu_i(\mathbf{B}_i - \mathbf{A}_i) \\ \sum_{i=1}^{n} \mathbf{P}_i^{-1}\mathbf{M}_i = n\mathbf{Q} \end{cases} \tag{18}$$

and this can also be re-arranged into matricial form as follows:

$$\mathbf{y} = \mathbf{Kx} \tag{19}$$

with:

$\mathbf{y} = [\mathbf{Q}, \mu_1, \cdots, \mu_n]^T$,

$\mathbf{x} = \left[\mathbf{A}_1^T(\mathbf{B}_1 - \mathbf{A}_1), \cdots, \mathbf{A}_n^T(\mathbf{B}_n - \mathbf{A}_n), \sum_{i=1}^{n} \mathbf{P}_i^{-1}\mathbf{A}_i\right]^T$,

and the matrix $\mathbf{K}$ is equal to:

$$\begin{bmatrix} (\mathbf{B}_1 - \mathbf{A}_1)^T\mathbf{P}_1 & -\left\|\mathbf{B}_1 - \mathbf{A}_1\right\|^2 & 0 & \cdots \\ \vdots & 0 & \ddots & 0 \\ (\mathbf{B}_n - \mathbf{A}_n)^T\mathbf{P}_n & \vdots & 0 & -\left\|\mathbf{B}_n - \mathbf{A}_n\right\|^2 \\ n\mathbf{I} & -\mathbf{P}_1^{-1}(\mathbf{B}_1 - \mathbf{A}_1) & \cdots & -\mathbf{P}_n^{-1}(\mathbf{B}_n - \mathbf{A}_n) \end{bmatrix}.$$

Finally, equation (18) is solved according to:

$$\mathbf{x} = \left(\mathbf{K}^T\mathbf{K}\right)^{-1}\mathbf{K}^T\mathbf{y}. \tag{20}$$

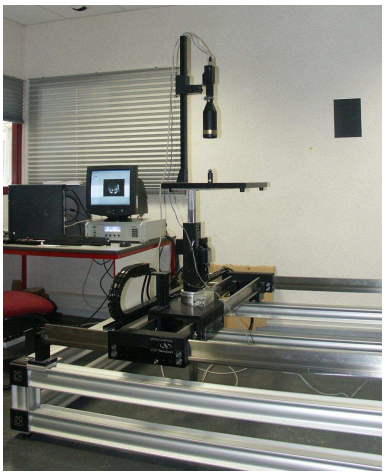

Fig. 6. Experimental set up.

## V. Experimental Results

The experimental set up is presented Fig. 6. The imaging system is made of a CCD camera with a telecentric lens, and a hyperbolic mirror. In order to precisely control its displacement, we have placed it on a precision three axes stage. The $x \times y \times z$ operating area is $1.5m \times 1.6m \times 0.4m$ and the $x \times y \times z$ room size is about $6m \times 5m \times 2.5m$. After calibrating our catadioptric sensor by polarization imaging, we have triangulated 3D points of interest by moving the system. We present preliminary results of the three-dimensional reconstruction of the points with the pixel-ray model and the two previously introduced triangulation methods.

### A. Validation of the calibration

Since, there is no parametric model of our imaging system, the validation of the calibration is performed by comparing the result of the mirror reconstruction to its theoretical shape which is given by its surface equation:

$$\frac{z^2}{789.3274} - \frac{x^2 + y^2}{548.1440} = 1. \tag{21}$$

To calibrate the system, the rotating polarizer is placed between the lens and the mirror, and a white paper sheet cylinder around the mirror. After automatically computing the polarization parameters, by knowing the refractive index of the material, the calibration is directly done for every pixel. Fig. 7 shows the error map of the reconstruction of the hyperbolic mirror. An important error occurs in the top of the mirror where the normals are oriented near the optical axis. In the mirror region of interest (the annulus bounded by the mirror contour and a small circle excluding the image center), the reconstruction gives accurate results with an average error less than $0.1mm$ (the mirror diameter is $60mm$).

### B. Preliminary results

Once the imaging system is calibrated, three images with three different known positions have been acquired. We pick several points of interest on each images such as

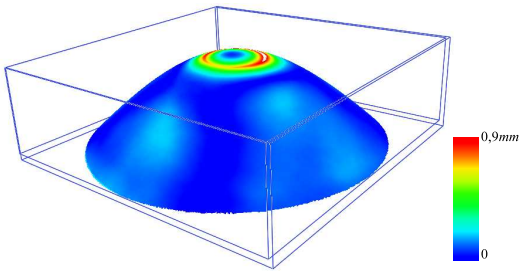


Fig. 7. Error map of the reconstruction of the hyperbolic mirror.

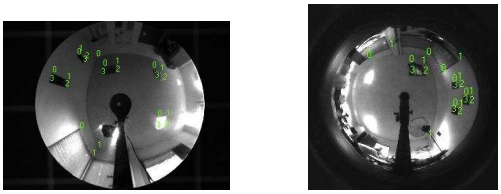

(a) (b)

Fig. 8. Picking of points of interest on the (a) hyperbolic and (b) spherical mirror.

two rectangular targets, one edge of the ceiling, one edge of the top of the window and three fluorescent lightings (Fig. 8(a)). The result of the triangulation process for the hyperbolic mirror is presented Fig. 9. It can be seen that the reconstruction is qualitatively satisfactory. The global topology of the scene and the relative distances are respected; right angles appear as (near-) right angles. In fact, the overall reconstruction is as expected, considering:

- the small displacement of the sensor by comparison with the size of the scene;
- the fact that we only performed linear triangulation without refinement;
- the reconstruction depends also on the accuracy of point picking (the correspondence has been established manually and a slight error in the location of 2D points lead to erroneous 3D reconstruction).

Reconstruction with a spherical mirror was also performed. The points that were selected represent three rectangular targets, one fluorescent lighting, one horizontal and one vertical windows edges (Fig. 8(b)). Even though the mirror curvature is higher, the results are comparable to the ones obtained with the hyperbolic mirror (Fig. 10).

## VI. Conclusion and Future Work

In this paper, a new efficient method of calibration for catadioptric sensors has been presented. This method is based on the pixel-ray model recently proposed by Sturm [1].

The calibration can be performed "in one click" even by a non-specialist as it only requires an optical apparatus, no image processing and no calibration pattern. It deals with misalignment of the sensor and work for any shape of mirror (regular or not). Experimental results prove that the sensor is properly calibrated and a satisfactory three-dimensional reconstruction of the scene could be obtained from it. However, the mapping between image pixels and projection rays

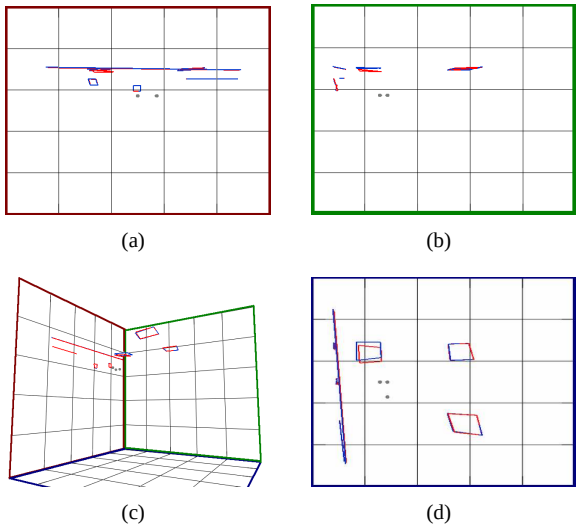

(a) (b) (c) (d)

Fig. 9. Triangulation results of the hyperbolic mirror, (a) view direction towards $X-Y$ plane, (b) view direction towards $Y-Z$ plane, (c) three-dimensional view, (d) view direction towards $X-Z$ plane.

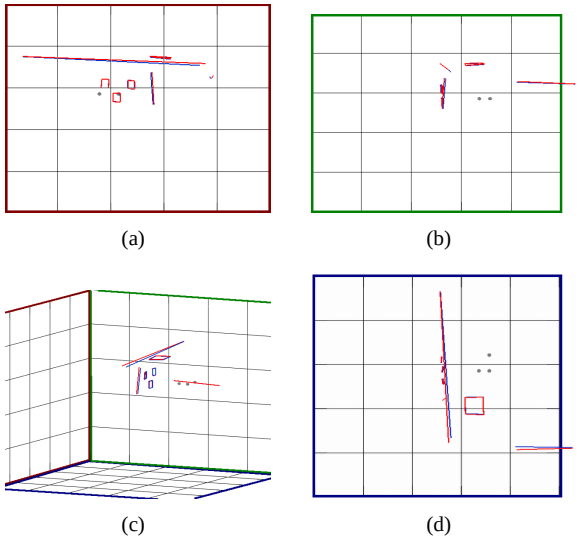

(a) (b) (c) (d)

Fig. 10. Triangulation results of the spherical mirror, (a) view direction towards $X-Y$ plane, (b) view direction towards $Y-Z$ plane, (c) three-dimensional view, (d) view direction towards $X-Z$ plane.

can only be computed so far with an orthographic camera (i.e. a telecentric lens). As a future work, we propose to further develop the method (calibration *and* reconstruction) by improving it by:

- generalizing the pixel-ray mapping to perspective cameras;
- quantifying the robustness of the calibration method by analyzing the influence of noise on the reconstruction;
- refining the triangulation by means of bundle adjustment (this is a key point because there is no parametric model of projection for such model so that it is not that simple to minimize a 2D residual error!).

## VII. Acknowledgments

The authors would like to thank the whole staff of *Plateform3D - Le Creusot* (http://www.plateform3d.com) for kindly providing us with the hyperbolic mirror.

## References

[1] P. Sturm, "Multi-view geometry for general camera models," in *CVPR '05: Proceedings of the 2005 IEEE Computer Society Conference on Computer Vision and Pattern Recognition (CVPR'05) - Volume 1*, (Washington, DC, USA), pp. 206–212, IEEE Computer Society, 2005.

[2] M. D. Grossberg and S. K. Nayar, "A general imaging model and a method for finding its parameters," in *Eighth IEEE International Conference on Computer Vision, ICCV 2001*, vol. 2, pp. 108–115 vol.2, 2001.

[3] R. Pless, "Using many cameras as one," in *Computer Vision and Pattern Recognition*, 2003.

[4] S. Ramalingam, S. K. Lodha, and P. Sturm, "A generic structure-from-motion framework," *Computer Vision and Image Understanding*, vol. 103, pp. 218–228, September 2006.

[5] L. B. Wolff, "Polarization-based material classification from specular reflection," vol. 12, pp. 1059–1071, November 1990.

[6] L. B. Wolff and T. E. Boult, "Constraining object features using a polarization reflectance model," vol. 13, pp. 635–657, July 1991.

[7] D. Miyazaki, M. Kagesawa, and K. Ikeuchi, "Transparent surface modeling from a pair of polarization images," vol. 26, pp. 73–82, January 2004.

[8] O. Morel, C. Stolz, F. Meriaudeau, and P. Gorria, "Three-dimensional inspection of highly-reflective metallic objects by polarization imaging," *Electronic Imaging Newsletter*, vol. 15, no. 2, p. 4, 2005.

[9] O. Morel, C. Stolz, F. Meriaudeau, and P. Gorria, "Active lighting applied to 3d reconstruction of specular metallic surfaces by polarization imaging," *Applied Optics*, vol. 45, pp. 4062–4068, June 2006.

[10] P. Sturm and S. Ramalingam, "A generic concept for camera calibration," in *Proceedings of the European Conference on Computer Vision, Prague, Czech Republic*, vol. 2, pp. 1–13, Springer, May 2004.

[11] R. Frankot and R. Chellappa, "A method for enforcing integrability in shape from shading algorithms," vol. 10, pp. 439–451, July 1988.

[12] R. Hartley, "Triangulation," *Computer Vision and Image Understanding*, vol. 68(2), pp. 146–157, 1997.